HHS Public Access

Author manuscript

Microsc Res Tech. Author manuscript; available in PMC 2019 January 29.

Published in final edited form as:

Microsc Res Tech. 2013 June ; 76(6): 625–632. doi:10.1002/jemt.22209.

Quantitative Zonal Differentiation of Articular Cartilage by Microscopic Magnetic Resonance Imaging, Polarized Light Microscopy, and Fourier-Transform Infrared Imaging

JI HYUN LEE and **YANG XIA***

Department of Physics and Center for Biomedical Research, Oakland University, Rochester, Michigan 48309

Abstract

This study aimed to synchronize the zonal differentiation of the full-thickness articular cartilage by three micro-imaging techniques, namely microscopic magnetic resonance imaging (μMRI), polarized light microscopy (PLM), and Fourier-transform infrared imaging (FTIRI). Eighteen cartilage-bone blocks from three canine humeral joints were imaged by: (a) μMRI T_2 relaxation at 0° and 55° orientations in a 7 T magnetic field, (b) PLM optical retardation and azimuthal angle, and (c) FTIRI amide I and amide II anisotropies at 0° and 90° polarizations relative to the articular surface. In addition, μMRI T_1 relaxation was imaged before and after the tissue being immersed in gadolinium (contrast agent) solution, to calculate the proteoglycan concentration. A set of previously established criteria in cartilage imaging was revised. The new criteria could simultaneously correlate the thicknesses of the three consecutive subtissue zones in articular cartilage among these imaging techniques.

Keywords

articular cartilage; anisotropy; μMRI; PLM; FTIRI; dichroic ratio

INTRODUCTION

Articular cartilage is a thin layer of soft tissue that protects the ends of bones in joints. The tissue contains mainly three types of molecules in its extracellular matrix: water, proteoglycans (PG) and collagen fibrils (Maroudas, 1975; Buckwalter and Mankin, 1998). Because of the structural orientation of its collagen fibrils, the noncalcified cartilage has been *conceptually* subdivided along its depth (thickness) into three subtissue zones, the superficial zone (SZ) where the fibrils are parallel to the articular surface, the transitional zone (TZ) where the fibrils are randomly oriented, and the radial zone (RZ) where the fibrils are perpendicular to the articular surface (Jeffery et al., 1991). As the degradation of articular cartilage is a hallmark of osteoarthritis and other forms of arthritis (Murphy et al., 2008), it is critical to understand the process of tissue degradation during its early stages

*Correspondence to: Yang Xia, Department of Physics, Oakland University, Rochester, Michigan 48309. xia@oakland.edu.

(before it becomes a clinical disease). As early lesions are small and localized, any effective evaluation of the joint diseases must have high resolution in nondestructive imaging.

Among the common micro-imaging techniques for cartilage research, three modalities are particularly important because of their unique capabilities (Xia, 2008). They are microscopic MRI (μMRI), polarized light microscopy (PLM), and Fourier-transform infrared imaging (FTIRI). MRI provides excellent soft tissue contrast and is widely used in clinics to diagnose human cartilage lesions (Mlynarik et al., 1999; Burstein et al., 2001; Eckstein et al., 2008). An important fact in MRI of articular cartilage is that the tissue can appear laminated when placed at certain orientations with respect to the magnetic field (B_0). This phenomenon, known as the magic angle effect in MRI of cartilage, is due to the fact that T_2 relaxation time in the tissue can be influenced by the dipolar interaction among the water molecules, which is depth-dependent because of the collagen structures in cartilage. Because of the thinness of the cartilage tissue, the resolution in clinical MRI (typically 0.4–0.6 mm per pixel) is insufficient to resolve any small lesion in human cartilage. Based on the same physics principle and engineering architectures, μMRI can have the transverse resolution as fine as tens of microns (Xia, 1998, 2007), exceptionally suitable for the study of cartilage degradation in animal models. A number of recent studies have demonstrated the importance of μMRI in the study of healthy and degraded cartilage (Xia, 1998; Bashir et al., 1999; Nieminen et al., 2000; Burstein et al., 2001; Cova and Toffanin, 2002; Alhadlaq et al., 2004).

Light microscopy is considered the gold standard in biomedicine. When the light is polarized, the birefringent property of the collagen fibrils in articular cartilage offers an opportunity to distinguish the individual zones in cartilage (Arokoski et al., 1996). One digital version of PLM (Oldenbourg and Mei, 1995; Xia et al., 2001) is capable of generating two quantitative maps, the angle map (in units of degree) and the retardation map (in units of nanometer). The value of angle measures the average orientation of all collagen fibrils within each voxel, where a nominal 90° difference is expected between SZ and RZ. The retardation represents the optical path difference between the electric and magnetic fields emerging from an anisotropic material and its value is indicative of the collagen organization within each voxel. Mapping these two parameters have permitted the detection of a disrupted collagen matrix due to the early onset of lesions and a tissue deformation due to loading (Xia et al., 2001; Alhadlaq et al., 2007; Rieppo et al., 2008).

FTIRI can sense various dipole vibrations in the specimen with a pixel resolution on the order of several microns. In the mid-infrared region, cartilage has several significant absorption peaks, such as amide I (C=O vibration at ~1,700–1,600 cm^{-1}) and amide II (C-N vibration at ~1,600–1,500 cm^{-1}) (Camacho et al., 2001; Potter et al., 2001). Similar to the polarization of visible light in PLM, the infrared light can also be polarized, which can be used to study the anisotropy of these dipole bonds (Ramakrishnan et al., 2007a; Xia et al., 2007). Since the amide components in articular cartilage are highly depth-dependent, the dichroic ratio ($DR = A_{//}/A_{\perp}$, where $A_{//}$ and $A_{\perp}$ represent the IR absorptions at the parallel and perpendicular polarizations, respectively), which is sensitive to the molecular orientation (Ramakrishnan et al., 2007a; Yin et al., 2011), is a useful parameter in FTIRI anisotropy studies. Recent FTIRI studies of cartilage included the chemical visualization (Gadaleta et al., 1996; Bi et al., 2005), quantification of the chemical concentrations (Camacho et al.,

2001; Kim et al., 2005), the amide anisotropy (Ramakrishnan et al., 2007a; Xia et al., 2007), and the depth-dependent changes in the amide anisotropy due to cartilage deformation (Xia et al., 2008a).

Although these imaging techniques had been used individually to study articular cartilage, the quantitative correlations among all three techniques had never been simultaneously established based on the same tissue. As these imaging tools are based on different physical mechanisms (the motional anisotropy of protons in μMRI, the optical birefringence in PLM, and the vibrational anisotropy of amide absorption in FTIRI), these imaging techniques are complementary to each other. It would be useful to establish the simultaneous correlations among them in articular cartilage at microscopic resolution. As it would be impractical to routinely use all imaging techniques together in any project, the establishment of these multidisciplinary correlations could be used to suggest the potential implications when only one technique is being used. These were the motivations of this comprehensive imaging project. The specific aims of this study were to quantify the zonal boundaries of articular cartilage and to correlate the subtissue zones simultaneously among these three imaging techniques. The accurate definition of these subtissue zones would be an important step toward the understanding of the structural properties of this load-bearing tissue and the loss of load-bearing ability of cartilage in common disease such as osteoarthritis.

MATERIALS AND METHODS

Cartilage Sample

Three humeral heads were harvested from the right shoulder joints of three healthy and mature canines (male, 1–2-years-old), which were sacrificed for an unrelated and approved study. A total of eighteen blocks were used in this study—six from the central load-bearing region of each fresh joint (Fig. 1). Each block contained the full-thickness cartilage that was still attached to the underlying bone and was approximately $1.75 \times 2 \times 3.5\ mm^3$. These fresh tissue blocks were immersed in saline with 1% protease inhibitor cocktail (P2714, Sigma, St. Louis, MO) at 4°C. The maximum storage time for any block was less than 72 h after harvesting.

μMRI Method

The microscopic magnetic resonance imaging (μMRI) experiments were performed using a Bruker AVANCE || 300 μMRI system (Bruker Instrument, Billerica, MA). All experiments used the magnetization-prepared imaging protocols that were documented earlier (Xia et al., 1997, 2008b). To obtain the glycosaminoglycan (GAG) image, the dGEMRIC protocol was followed (Bashir et al., 1999; Xia et al., 2008b). Specifically, one block from each animal was T_1-imaged when the block was soaked in saline and oriented at 55° with respect to the magnetic field. Subsequently, all eighteen blocks were T_1-imaged at 55° after being immersed in a 1 mM Gd-DTPA solution for 10 h. A GAG image was then calculated for each specimen (Xia et al., 2008b). The T_1-imaging sequence had a repetition time of either 1.5 or 0.5 s for before or after the block was soaked in the Gd solution, respectively. The T_1 contrast segment had five increments using 0, 0.4, 1.1, 2.2, and 4.0 s before the Gd immersion and 0, 0.1, 0.3, 0.5, 1.0 s in the Gd solution.

After the T_1 experiments, all eighteen blocks were T_2-imaged twice at 0° and 55° to the magnetic field, where the dipolar interaction was maximized (at 0°) and minimized (at 55°) respectively (Xia et al., 1997). The echo times for the T_2-contrast varied five times (at 0°: 2, 4, 10, 30, and 60 ms; at 55°: 2, 14, 36, 60, and 120 ms), while the 2D imaging echo time was fixed at 7.2 ms. The repetition time was 0.5 s. Both T_1 and T_2 were calculated by fitting of the images mono-exponentially on a pixel-by-pixel basis. The in-plane resolution was 12.5 μm and the slice thickness was 1 mm (Xia et al., 1997, 2008b). Other experimental parameters followed the previous work in the literature (Xia et al., 1997, 2008b).

Histological Method for PLM & FTIRI

After the nondestructive μMRI experiments, all tissue blocks were cut approximately at the same location of the imaging slice so that the same plane that had been imaged by μMRI could be studied by optical imaging. To identify the end of the imaging plane, a marker was created on each half of the block. The specimens were fixated, decalcified and paraffin embedded using the standard procedures (Xia et al., 2001). The embedded blocks were sectioned into 6-μm thin sections, which were mounted onto MirrIR slides (Kevley, Chesterland, OH) to allow the simultaneous imaging of the same cartilage section by both PLM and FTIRI (Xia et al., 2007, 2008a). Ten to fourteen sections were made from each of 18 blocks, each containing the full thickness tissue still attached to the underlining bone. At least three good-quality sections from each block were imaged using PLM and FTIRI. Other experimental details followed the documentation in the literature (Xia et al., 2001).

PLM Method

The PLM system consists of a digital imaging attachment (Cambridge Research & Instrumentation, Woburn, MA) mounted on a polarized light microscope (Leica DMRXP, Wetzlar, Germany) (Xia et al., 2001). The output of the CCD camera was processed according to a published algorithm (Oldenbourg and Mei, 1995), which generated two quantitative images of the optical retardance and the angular orientation. All specimens were imaged at the identical orientation with a 5× objective, which yielded an isotropic pixel size of 2.0 μm. Other experimental details were documented earlier in the literature (Xia et al., 2001).

FTIRI Method

The infrared images were acquired using a PerkinElmer Spotlight-300 infrared imager (Wellesley, MA). A rectangular ROI, approximately 156 × 943 μm^2, was imaged from each tissue section, using the reflection mode and an 8 cm^{-1} spectral interval (Xia et al., 2007). (This ROI was approximately the same size and at the same location of the μMRI slices. Imaging a ROI instead of the whole section shortened the total experimental time). An IR polarizer was inserted between the sample and the detector, at two polarization states of 0° and 90°: 0° ($A_{//}$) was aligned parallel to the articular surface while 90° ($A_{\perp}$) was aligned perpendicular to the articular surface. The 2D amide I and amide II maps were extracted using the PerkinElmer software (Xia et al., 2007). The nominal pixel resolution was 6.25 μm. Other experimental details were documented earlier in the literature (Xia et al., 2007).

Data Analysis

The results are presented as both 2D images and 1D cross-sectional profiles. The signal-to-noise ratio of the 1D profiles was enhanced by averaging parallel neighboring columns of the ROI to calculate an averaged depth-dependent profile with the standard deviation, using KaleidaGraph (Synergy Software, Reading, PA). Each technique used approximately the same ROI (~125 μm wide) at the same tissue location. Since the averaging process occurred perpendicular to the cartilage depth, the pixel resolutions of the 1D profiles along the direction of the cartilage depth in each technique were still 12.5, 2.0, and 6.25 μm, for μMRI, PLM, FTIRI respectively.

RESULTS

The μMRI Results

In articular cartilage, T_1 is known to be isotropic and changes in small amount in the depth profiles (Xia, 1998; Xia et al., 2008b). The T_1 mapping was hence only at 55°, which was used to calculate the GAG images by μMRI. T_2 in cartilage by comparison is known to be strongly anisotropic and changes significantly in the depth profiles (Xia, 1998; Xia et al., 2008b). The T_2 mapping was done both at 0° for the division of the subtissue zones and at 55° (the magic angle) for the determination of the total thickness of articular cartilage. A representative set of the μMRI results are shown in Figure 2a. The first intensity images at 55° were used to measure the total tissue thickness, which was 669 ± 62 μm based on all 18 blocks.

The averaged T_1 profile in Figure 3a clearly showed the $T_{1\text{-before}}$ was nearly independent of the tissue depth. The 2D GAG concentration profile, based on both $T_{1\text{-before}}$ and $T_{1\text{-after}}$ images, showed the GAG concentration as a linear gradient of the tissue depth (Xia et al., 2008b). The averaged GAG by μMRI was 74 ± 22 mg/mL, which was consistent to the bulk GAG (65 ± 7 mg/mL, which was the average of nineteen specimens that were measured from the previous histochemical study (Xia et al., 2008b)). Note that the animals in this study and in the separate histochemical study (Xia et al., 2008b) were from the same source —the animals had the identical species, age, and health status. The errors in the GAG value by μMRI reflected the fact that this GAG value by μMRI was the average of a spatially resolved profile. In comparison, the GAG value in the histochemical analysis came from a bulk assay, hence appeared to have smaller errors. The average T_2 profiles in Figure 3b clearly showed that the T_2 value was strongly dependent on both the cartilage depth and orientation in the magnetic field.

The PLM Results

A representative set of PLM images is shown in Figure 2b for the visible, angle and retardation images, whose depth-dependent profiles in Figure 3c illustrated several features of the angle and retardation images. (1) The angle map demonstrated the orientation change of the collagen fibrils, which was expected between SZ and RZ. (2) The larger errors in TZ of the angle profile (Figure 3c) illustrated an increased randomness among the fibrils when they were making the orientational transition. Note that the well-accepted concept of a 90° change in the fibril orientation between SZ and RZ still leaves the freedom for the surface

fibers to distribute themselves in any orientation in the 2D plane that is parallel with the articular surface, hence the notation of “surface fibril ambiguity” in the MRI literature (Xia et al., 2002; Zheng and Xia, 2009). In any angle image by PLM, consequently, the difference of the angles between SZ and RZ does not have to be exactly at 90°, which can be seen in Figure 3c.

The 2D retardation images had a nonzero minimum value at the center of TZ, where the fibrils made the orientational change (Xia et al., 2001). The average value of this minimum retardation from all 18 blocks was 0.7 ± 0.2 nm at the depth of 80 ± 25 μm. As a comparison, the averaged value of the background retardation was 0.43 ± 0.02 nm. The difference was significant, which demonstrated that a residual organization of the collagen fibrils existed even in the most random location of the cartilage. The tidemark that separated the noncalcified and calcified regions in cartilage was recognizable as a faint line in the retardation image in Figure 2c, which coincided with the maximum of the retardation value in the profile at the deep tissue in Figure 3c. However, the tidemark was not visible in the angle images, which implied that the fibril orientation remained relatively constant from the uncalcified to the calcified tissue. The averaged surface-to-tidemark thickness by PLM from 18 blocks was 646 ± 49 μm.

The FTIRI Results

As FTIRI data has the true 3D hyperspectral image format (two spatial dimensions in μm and one chemical dimension in cm^{-1}), the absorbance maps at different wavenumbers can be extracted from a single FTIRI experiment. Figure 2c showed the amide I and II maps at the polarizations of 0° and 90°. When the long axis of the fibrils was in the plane of the tissue section, the bond directions of amide I and amide II were approximately perpendicular and parallel to the fibril axis respectively (Camacho et al., 2001; Xia et al., 2007). A quantitative way to represent the amide anisotropies was the calculation of the dichroic ratios, which was shown in Figure 3d. These two DR profiles used all specimens from 18 blocks, where a crossover point between the DR1 (DR for amide I) and DR2 (DR for amide II) was clearly visible at an averaged depth of 71 ± 25 μm.

Characteristics of Articular Cartilage by μMRI, PLM, and FTIRI

Table 1 summarized the characteristics of canine humeral articular cartilage from all three imaging experiments, which serves as the reference for this type of tissue. To reach a set of criteria that are capable of simultaneously subdividing the zones, three quantitative profiles were examined in detail: the asymmetrically bell-shaped T_2 profiles at 0° in MRI, the angle profiles in PLM, and the dichroic ratios of amide anisotropy in FTIRI (Fig. 3). Table 2 summarized the methods of the new criteria that could simultaneously correlate the subtissue zones in articular cartilage by μMRI, PLM, and FTIRI.

The new μMRI criterion was based on the first derivative of the T_2 profile at 0° (Fig. 4a), which was found to be more sensitive to the T_2 changes than the previous value-based μMRI criterion (Xia, 1998; Xia et al., 2001). The maximum of the first derivative of T_2 was chosen as the boundary between SZ and TZ, and the minimum of the first derivative of T_2 was chosen as the boundary between TZ and RZ.

The new PLM criterion was based on the first derivative of the angle profile (Fig. 4b), which was found to provide better correlation than the previous value-based PLM criterion (Xia et al., 2001). The full-width-half-maximum (FWHM) of the first derivative was used to define the thickness and location of TZ. The SZ and the RZ could be subsequently determined once the TZ was established.

The new FTIRI criterion was based on the previously established features of the DR1 and DR2 profiles (Fig. 4c) (Ramakrishnan et al., 2007b), with a different percentage of the deviation. As the dichroic ratios cross each other at the unity in the middle of TZ, it was found during this project that a 5% deviation from the unity on both DR1 and DR2 was able to determine the location and thickness of the TZ.

The results of the zone divisions from all three imaging techniques were summarized in Table 3, together with the p-probabilities from the one-way ANOVA ($N = 18$ each). All three zones were not significantly affected among the three techniques with the P values (95%, if $P < 0.05$, it is significantly different among the three techniques) of 0.376 for the SZ, 0.117 for the TZ, and 0.260 for the RZ. In addition, the depth of the most random location in articular cartilage could also not be affected with significance ($P = 0.783$) among the imaging techniques (Table 3), which is shown in Figure 5 as the linear regression plots.

DISCUSSIONS

Even though the qualitative description of the subtissue zones in cartilage is well accepted, the quantitative division of the whole tissue into the sub-tissue zones is less clear (Maroudas et al., 1980; Xia, 2007; Hannila et al., 2009). Furthermore, a simultaneous correlation among these important micro-imaging techniques was unknown. As these imaging tools were becoming widely used in cartilage research, the need of a quantitative correlation was persuasive. As the early cartilage lesion can only be visualized by microscopic imaging, the identification of the subtissue zones in cartilage and the correlation of these zones among different micro-imaging techniques were considered vital.

The Criteria that Subdivide the Tissue Zones in Articular Cartilage

Please note that the definition of “subtissue zone” in cartilage is only a concept (Xia, 2008). Anyone who uses high-resolution imaging to examine a piece of articular cartilage will not find any abrupt “line” or “border” separating any two different zones inside the tissue. Any change in the tissue’s property is always gradual over a finite distance. Consequently, the criteria to truncate a tissue into several discrete zones are intrinsically arbitrary (Xia, 2008). However, this concept of the ‘discrete zones’ is useful, which conveniently draws one’s attention to a particular depth of tissue. The motivation of the zone division in this project was to seek a set of quantitative criteria, one for each imaging tool, which could divide the tissue into the conceptual zones whose thicknesses were mutually correlated among these imaging tools. Such correlation will benefit any future comprehensive or collaborative project that requires different tools or multiple labs. Although these criteria might seem subjective, each set of criterion was based on solid physical mechanisms. Even though a tissue other than canine humeral cartilage could have different values in the criteria, the general approach should be informative for future work.

The μMRI criterion was based on the T_2 profile at 0°, where the water molecules in cartilage had the strongest dipole interaction with the magnetic field. In the past, the FWHM of the T_2 peak was used to subdivide the tissue into the zones (Xia et al., 2001). A more accurate correlation between μMRI and PLM was found in this project when the first derivative profile of T_2 at 0° was used (Fig. 4a), which measured the rate of the T_2 changes. The zone thicknesses by the previous value-based criterion were 44 ± 13 μm for SZ, 81 ± 12 μm for TZ, and 544 ± 69 μm for RZ, which overestimated the thicknesses of both SZ and TZ and underestimated the thickness of RZ.

The PLM criterion was based on the angle profile, which shows an approximate 90° difference between SZ and RZ. In the past, an angle deviation from the fitted angle profile by more than 1° was used to define the TZ in PLM (Xia et al., 2001). In this project, the use of the first derivative of the fitted angle profile (Xia, 2008) (Fig. 4b) was found to provide a better correlation among all imaging techniques. The bigger changes in the derivative profile also made it easier to define the TZ boundaries. The zonal thicknesses by the previous value-based criteria were 46 ± 22 μm for SZ, 63 ± 14 μm for TZ, and 537 ± 66 μm for RZ, which overestimated the thickness of TZ and underestimated the thicknesses for both SZ and RZ.

The FTIRI criterion was based on the dichroic ratio profiles of amide I and amide II. A two-step polarization study provided a crossover of its dichroic ratios at the most random location of the tissue section. In the past, the FTIRI criterion was based on the 3% deviation of the DR1 and DR2 profiles (Ramakrishnan et al., 2007b). In this project, it was found that a 5% deviation to the crossover enabled a better correlation between the chemical zones from FTIRI and the zones from other imaging tools. The zone thicknesses by the previous criterion were 56 ± 22 μm for SZ, 36 ± 9 μm for TZ, and 626 ± 65 μm for RZ, which underestimated the thickness of the TZ and overestimated the thicknesses of both SZ and RZ.

The Most Random Location in Articular Cartilage

As each imaging technique has its own physical mechanism, the definition of the most random location in articular cartilage (where the signal, or tissue structure, is the most random) depends upon the particular mechanism that the imaging technique employs. For μMRI, the location of the T_2 maximum (at 0°) defines the location at which the dynamic motion of the water molecules is most isotropic. For PLM, the location of the retardation minimum defines the depth where the largest fraction of the collagen fibrils is oriented close to 45°. For FTIRI, it is the vibration of the dipole bonds that defines the most random location in articular cartilage. The accurate identification of this location is important since a lesioned tissue is known to have a disturbed fibril structure, hence a modified random depth could signal a certain stage of the pathology in degradation. Possible reasons for a slightly weaker correlation between μMRI and the optical imaging could be (1) the influence of the (comparatively) large voxel in μMRI (Xia, 2007), which was shown to influence the locations of the T_2 peaks (Xia et al., 2002; Zheng and Xia, 2009) and (2) since the maximum T_2 is influenced by water content, the local water concentrations (such as ions, cell density, etc.) also plays a role, that provide relaxation mechanisms without reducing water mobility or motion isotropy. In addition, the orientation of the 2D tissue section from a 3D tissue

block could also influence the location of the retardation minimum in optical imaging (Mittelstaedt et al., 2011).

For any multidisciplinary correlation project, it would be natural to ask the question, if one does not have the time or equipment to use all of the techniques, when it is advantageous to use which imaging tool? A unique answer to this question probably does not exist, since the answer would be different for different situations. However, some general trends could be summarized. Among the three micro-imaging tools, μMRI has the lowest voxel resolution. However, μMRI plays the indispensable role in any biomedical research since μMRI has the same physics principles and engineering architectures as in clinical MRI, which is the gold standard in noninvasive soft-tissue imaging in hospitals. Hence, any invasive imaging would need to correlate with μMRI, to gain an entrance to the in vivo detection by clinical MRI. Between the two optical micro-imaging tools, PLM is inexpensive and its results (angle and retardation) have direct morphological meanings. In addition, PLM has superior image resolution because of its use of visible light. In comparison, the use of infrared light limits the spatial resolution in FTIRI. However, FTIRI plays a unique role since it is a chemical imaging tool and can, in principle, construct the 2D chemical maps of the specimens (David-Vaudey et al., 2005). For any disease where the molecular or chemical concentration change is an early sign, FTIRI should be a useful tool in the animal model research since it could image the early variations of the molecular concentration.

In this project, the individual zone thicknesses and locations in articular cartilage were established quantitatively and simultaneously, with statistical significances. To the best of our knowledge, this is the first quantitative study of articular cartilage utilizing μMRI, PLM, and FTIRI at microscopic resolutions. Although all individual methods had been used before in cartilage study, this project brought them together in cartilage research with a set of revised criteria in zone-division. Even though the physical mechanisms of these imaging tools are distinctly different, this set of revised criteria successfully defined the subtissue zones that were common among all imaging results. Although only canine humeral cartilage was studied in this project, the general approaches established in this project should be applicable for the study of other tissue. The potentials to associate three unique aspects of the tissue physically, morphologically and chemically from multidisciplinary imaging were demonstrated, which could enhance future clinical research and practice.

ACKNOWLEDGMENTS

The authors are grateful to Drs C. Les and H. Sabbah (Henry Ford Hospital, Detroit) for providing the canine joints, and Ms J. Spann (Michigan Resonance Imaging, Rochester Hills, MI) for providing the contrast agent. The authors are also grateful to Dr S. Zheng (current address: University of Massachusetts, Worcester, MA) and Dr M. Szarko (current address: University of London, UK) for technical help during the early stage of this project, and Mr. F. Badar for a MatLab code in relaxation calculation. The editorial comments by Mr D. Mittelstaedt and Ms C. Searight (both at Oakland University) and Dr S. Bowyer (Henry Ford Hospital, Detroit) are appreciated.

Contract grant sponsor: NIH R01; Contract grant number: AR045172 and AR052353.

REFERENCES

Alhadlaq HA, Xia Y, Hansen FM, Les CM, Lust G. 2007 Morphological changes in articular cartilage due to static compression: Polarized light microscopy study. Connect Tissue Res 48:76–84. [PubMed: 17453909]

Alhadlaq HA, Xia Y, Moody JB, Matyas JR 2004 Detecting structural changes in early experimental osteoarthritis of tibial cartilage by microscopic magnetic resonance imaging and polarised light microscopy. Ann Rheum Dis 63:709–717. [PubMed: 15140779]

Arokoski JP, Hyttinen MM, Lapvetelainen T, Takacs P, Kosztaczky B, Modis L, Kovanen V, Helminen H. 1996 Decreased birefringence of the superficial zone collagen network in the canine knee (stifle) articular cartilage after long distance running training, detected by quantitative polarised light microscopy. Ann Rheum Dis 55:253–264. [PubMed: 8733443]

Bashir A, Gray ML, Hartke J, Burstein D. 1999 Nondestructive imaging of human cartilage glycosaminoglycan concentration by MRI. Magn Reson Med 41:857–865. [PubMed: 10332865]

Bi X, Li G, Doty SB, Camacho NP. 2005 A novel method for determination of collagen orientation in cartilage by Fourier transform infrared imaging spectroscopy (FT-IRIS). Osteoarthritis Cartilage 13:1050–1058. [PubMed: 16154778]

Buckwalter JA, Mankin HJ. 1998 Articular cartilage: Tissue design and chondrocyte-matrix interactions. Instr Course Lect 47:477–486. [PubMed: 9571449]

Burstein D, Velyvis J, Scott KT, Stock KW, Kim YJ, Jaramillo D, Boutin RD, Gray ML. 2001 Protocol issues for delayed Gd(DTPA)(2-)-enhanced MRI (dGEMRIC) for clinical evaluation of articular cartilage. Magn Reson Med 45:36–41. [PubMed: 11146483]

Camacho NP, West P, Torzilli PA, Mendelsohn R. 2001 FTIR microscopic imaging of collagen and proteoglycan in bovine cartilage. Biopolymers 62:1–8. [PubMed: 11135186]

Cova M, Toffanin R. 2002 MR microscopy of hyaline cartilage: Current status. Eur Radiol 12:814–823. [PubMed: 11960232]

David-Vaudey E, Burghardt A, Keshari K, Brouchet A, Ries M, Majumdar S. 2005 Fourier Transform Infrared Imaging of focal lesions in human osteoarthritic cartilage. Eur Cell Mater 10:51–60; discussion 60. [PubMed: 16307426]

Eckstein F, Buck RJ, Burstein D, Charles HC, Crim J, Hudelmaier M, Hunter DJ, Hutchins G, Jackson C, Kraus VB, Lane NE, Link TM, Majumdar LS, Mazzuca S, Prasad PV, Schnitzer TJ, Taljanovic MS, Vaz A, Wyman B, Le Graverand MP. 2008 Precision of 3.0 Tesla quantitative magnetic resonance imaging of cartilage morphology in a multicentre clinical trial. Ann Rheum Dis 67:1683–1688. [PubMed: 18283054]

Gadaleta SJ, Landis WJ, Boskey AL, Mendelsohn R. 1996 Polarized FT-IR microscopy of calcified turkey leg tendon. Connect Tissue Res 34:203–211. [PubMed: 9023049]

Hannila I, Raina SS, Tervonen O, Ojala R, Nieminen MT. 2009 Topographical variation of T2 relaxation time in the young adult knee cartilage at 1.5 T. Osteoarthritis Cartilage 17:1570–1575. [PubMed: 19501682]

Jeffery AK, Blunn GW, Archer CW, Bentley G. 1991 Three-dimensional collagen architecture in bovine articular cartilage. J Bone Joint Surg Br 73:795–801. [PubMed: 1894669]

Kim M, Bi X, Horton WE, Spencer RG, Camacho NP. 2005 Fourier transform infrared imaging spectroscopic analysis of tissue engineered cartilage: Histologic and biochemical correlations. J Biomed Opt 10:031105. [PubMed: 16229630]

Maroudas A 1975 Biophysical chemistry of cartilaginous tissues with special reference to solute and fluid transport. Biorheology 12:233–248. [PubMed: 1106795]

Maroudas A, Bayliss MT, Venn M. 1980 Further studies on the composition of human femoral head cartilage. Ann Rheum Dis 39:514–534. [PubMed: 7436585]

Mittelstaedt D, Xia Y, Shmelyov A, Casciani N, Bidthanapally A. 2011 Quantitative determination of morphological and territorial structures of articular cartilage from both perpendicular and parallel sections by polarized light microscopy. Connect Tissue Res 52:512–522. [PubMed: 21787136]

Mlynarik V, Trattnig S, Huber M, Zembsch A, Imhof H. 1999 The role of relaxation times in monitoring proteoglycan depletion in articular cartilage. J Magn Reson Imaging 10:497–502. [PubMed: 10508315]

Murphy LST, Helmick CG, Renner JB, Tudor G, Koch G, Dragomir A, Kalsbeek WD, Luta G, Jordan JM. 2008 Lifetime risk of symptomatic knee osteoarthritis. Arthritis Rheum 59:1207–1213. [PubMed: 18759314]

Nieminen MT, Toyras J, Rieppo J, Hakumaki JM, Silvennoinen J, Helminen HJ, Jurvelin JS. 2000 Quantitative MR microscopy of enzymatically degraded articular cartilage. Magn Reson Med 43:676–681. [PubMed: 10800032]

Oldenbourg R, Mei G. 1995 New polarized light microscope with precision universal compensator. J Microscopy 180(Pt. 2):140–147.

Potter K, Kidder LH, Levin IW, Lewis EN, Spencer RG. 2001 Imaging of collagen and proteoglycan in cartilage sections using Fourier transform infrared spectral imaging. Arthritis Rheum 44:846–855. [PubMed: 11315924]

Ramakrishnan N, Xia Y, Bidthanapally A. 2007a Polarized IR microscopic imaging of articular cartilage. Phys Med Biol 52:4601–4614. [PubMed: 17634653]

Ramakrishnan N, Xia Y, Bidthanapally A, Lu M. 2007b Determination of zonal boundaries in articular cartilage using infrared dichroism. Appl Spectrosc 61:1404–1409. [PubMed: 18198035]

Rieppo J, Hallikainen J, Jurvelin JS, Kiviranta I, Helminen HJ, Hyttinen MM. 2008 Practical considerations in the use of polarized light microscopy in the analysis of the collagen network in articular cartilage. Microsc Res Tech 71:279–287. [PubMed: 18072283]

Xia Y 1998 Relaxation anisotropy in cartilage by NMR microscopy (μMRI) at 14-μm resolution. Magn Reson Med 39:941–949. [PubMed: 9621918]

Xia Y 2007 Resolution ‘scaling law’ in MRI of articular cartilage. Osteoarthritis Cartilage 15:363–365. [PubMed: 17218119]

Xia Y 2008 Averaged and depth-dependent anisotropy of articular cartilage by microscopic imaging. Semin Arthritis Rheum 37:317–327. [PubMed: 17888496]

Xia Y, Alhadlaq H, Ramakrishnan N, Bidthanapally A, Badar F, Lu M. 2008a Molecular and morphological adaptations in compressed articular cartilage by polarized light microscopy and Fourier-transform infrared imaging. J Struct Biol 164:88–95. [PubMed: 18634884]

Xia Y, Farquhar T, Burton-Wurster N, Lust G. 1997 Origin of cartilage laminae in MRI. J Magn Reson Imaging 7:887–894. [PubMed: 9307916]

Xia Y, Moody JB, Alhadlaq H. 2002 Orientational dependence of T2 relaxation in articular cartilage: A microscopic MRI (μMRI) study. Magn Reson Med 48:460–469. [PubMed: 12210910]

Xia Y, Moody JB, Burton-Wurster N, Lust G. 2001 Quantitative in situ correlation between microscopic MRI and polarized light microscopy studies of articular cartilage. Osteoarthritis Cartilage 9:393–406. [PubMed: 11467887]

Xia Y, Ramakrishnan N, Bidthanapally A. 2007 The depth-dependent anisotropy of articular cartilage by Fourier-transform infrared imaging (FTIRI). Osteoarthritis Cartilage 15:780–788. [PubMed: 17317225]

Xia Y, Zheng S, Bidthanapally A. 2008b Depth-dependent profiles of glycosaminoglycans in articular cartilage by microMRI and histochemistry. J Magn Reson Imaging 28:151–157. [PubMed: 18581328]

Yin JH, Xia Y, Ramakrishnan N. 2011 Depth-dependent anisotropy of proteoglycan in articular cartilage by fourier transform infrared imaging. Vib Spectrosc 57:338–341. [PubMed: 22025814]

Zheng S, Xia Y. 2009 The collagen fibril structure in the superficial zone of articular cartilage by microMRI. Osteoarthritis Cartilage 17:1519–1528. [PubMed: 19527808]

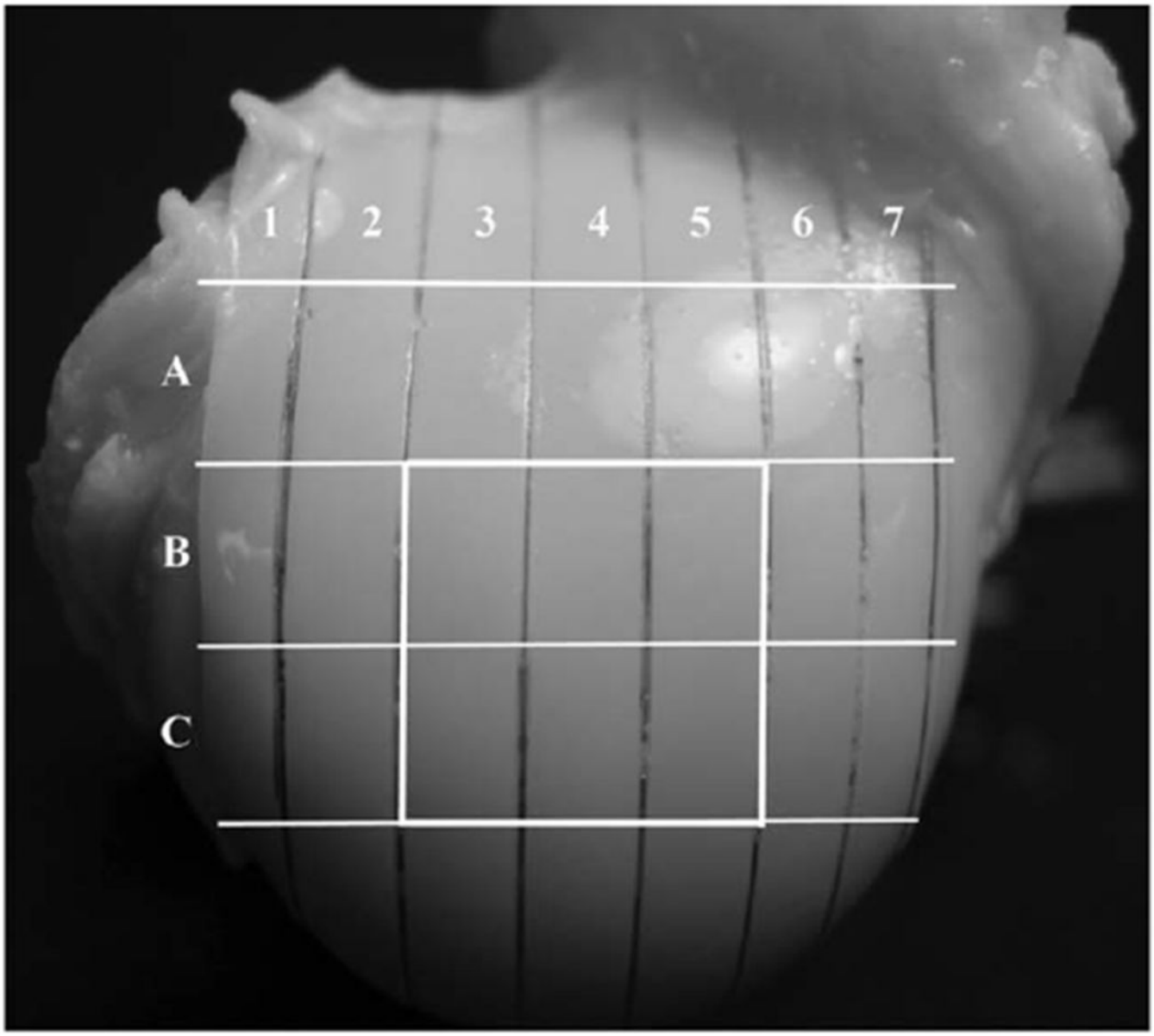

Fig. 1.

The locations of the tissue specimens on the surface of a humeral head. Six blocks (B3, B4, B5, C3, C4, C5) from each joint were imaged in this study.

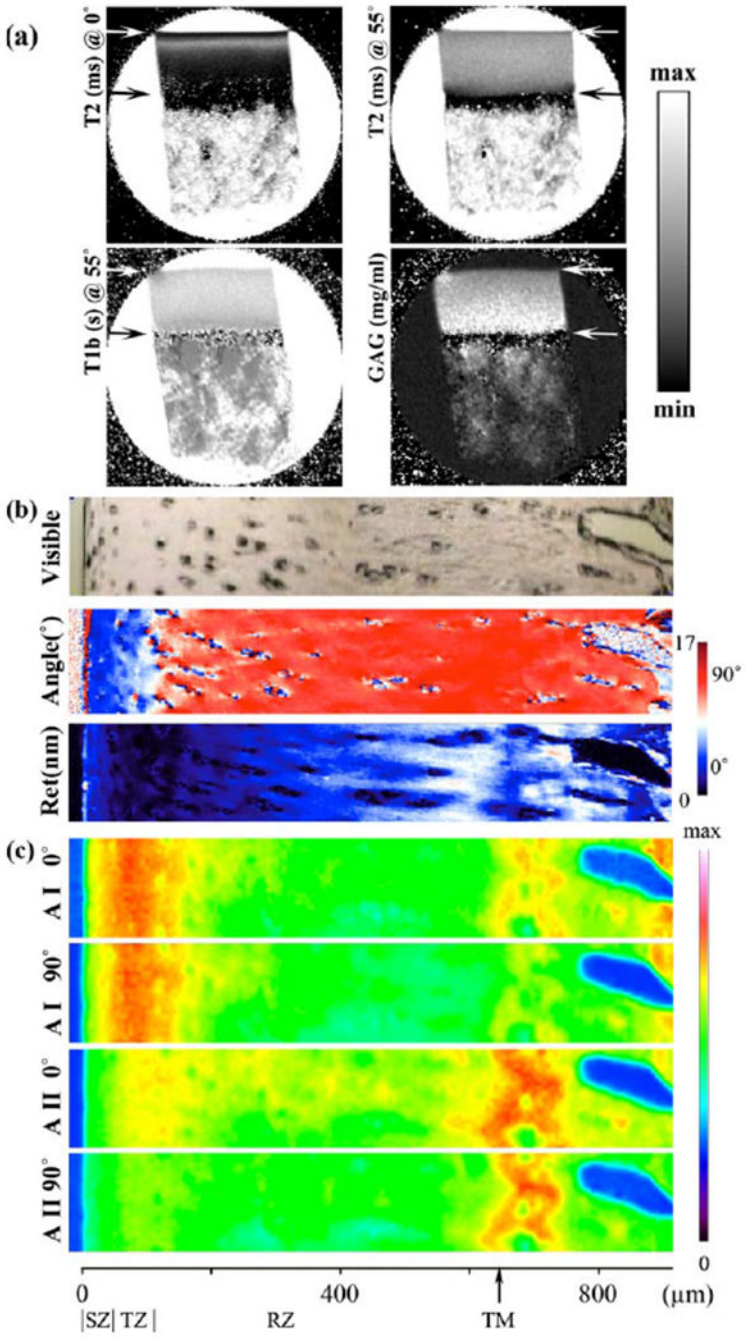

Fig. 2.

a: The 2D images of T_2 at 0° and 55° with respect to the magnetic field (vertically up), T_1 (at 55°) before soaked in Gd solution, and the GAG concentration. These μMRI images were plotted on a gray scale, with the minimum and maximum intensities set at 0–85 ms for T_2 (0°), 0–85 ms for T_2 (55°), 0–1.5 s for $T_{1\text{-before}}$, and 0–100 mg/mL for GAG, respectively. The upper arrow marked the boundary between cartilage and saline; the lower arrow marked the boundary between cartilage and bone. **b:** A visible image of the same specimen in (a) and two calculated PLM images: the angle image (45°–135°) and the retardation image (0–

17 nm). **c:** Four IR absorbance images from the selected area (156 μm by 943 μm) were labeled as AI (amide I) and AII (amide II) at 0° and 90°. The maximum absorbance for all images was 0.668. The horizontal scale indicated the thickness of the cartilage specimen in microns and was divided by the tissue zones. TM stands for the tidemark.

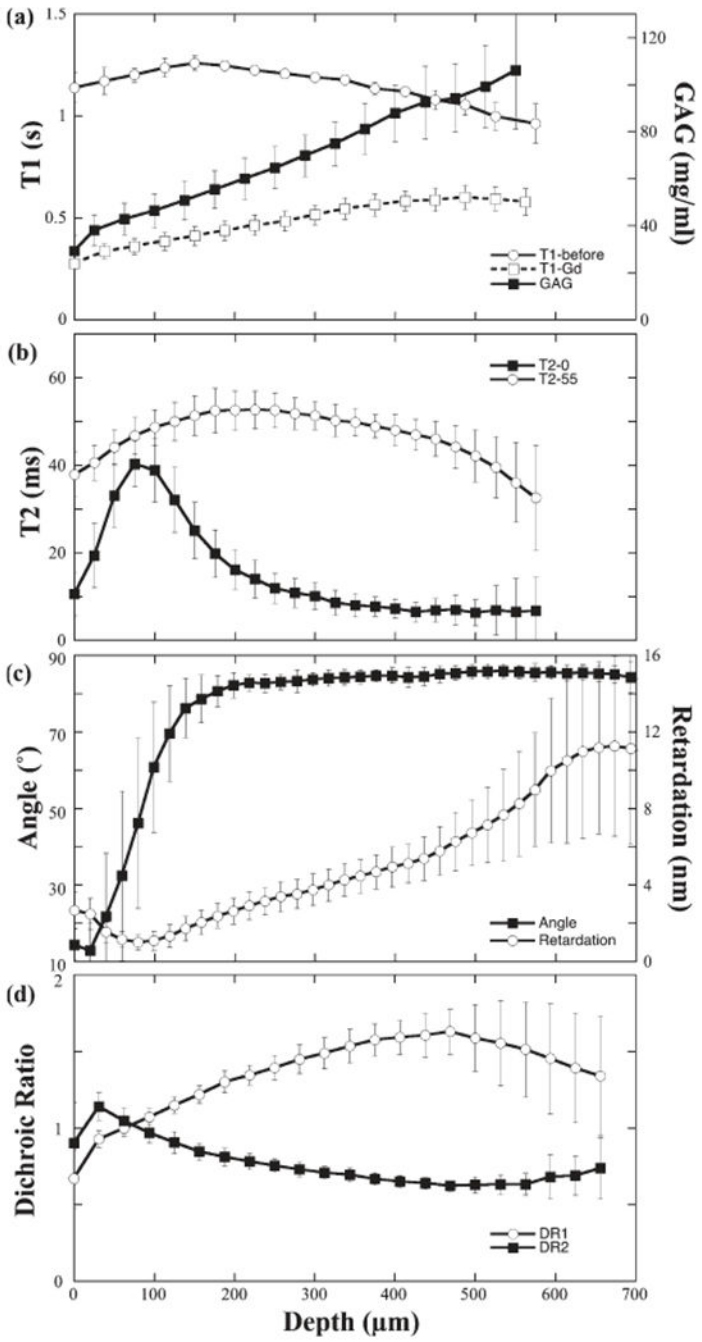

Fig. 3.

a: The averaged T_1 profiles before ($N = 3$) and after ($N = 18$) the specimens were immersed in the Gd solution, and the calculated GAG profile. **b:** The averaged T_2 profiles ($N = 18$, only one pixel in every two pixels was plotted) at two specimen orientations: 0° and 55°. **c:** The averaged profiles of optical retardation ($N > 36$) and angle ($N > 36$; only one pixel in every 10 pixels was plotted). **d:** The averaged dichroic ratio profiles of the amide I and II ($N > 36$, only one pixel in every five pixels was plotted). Error bars represented SD (standard deviations).

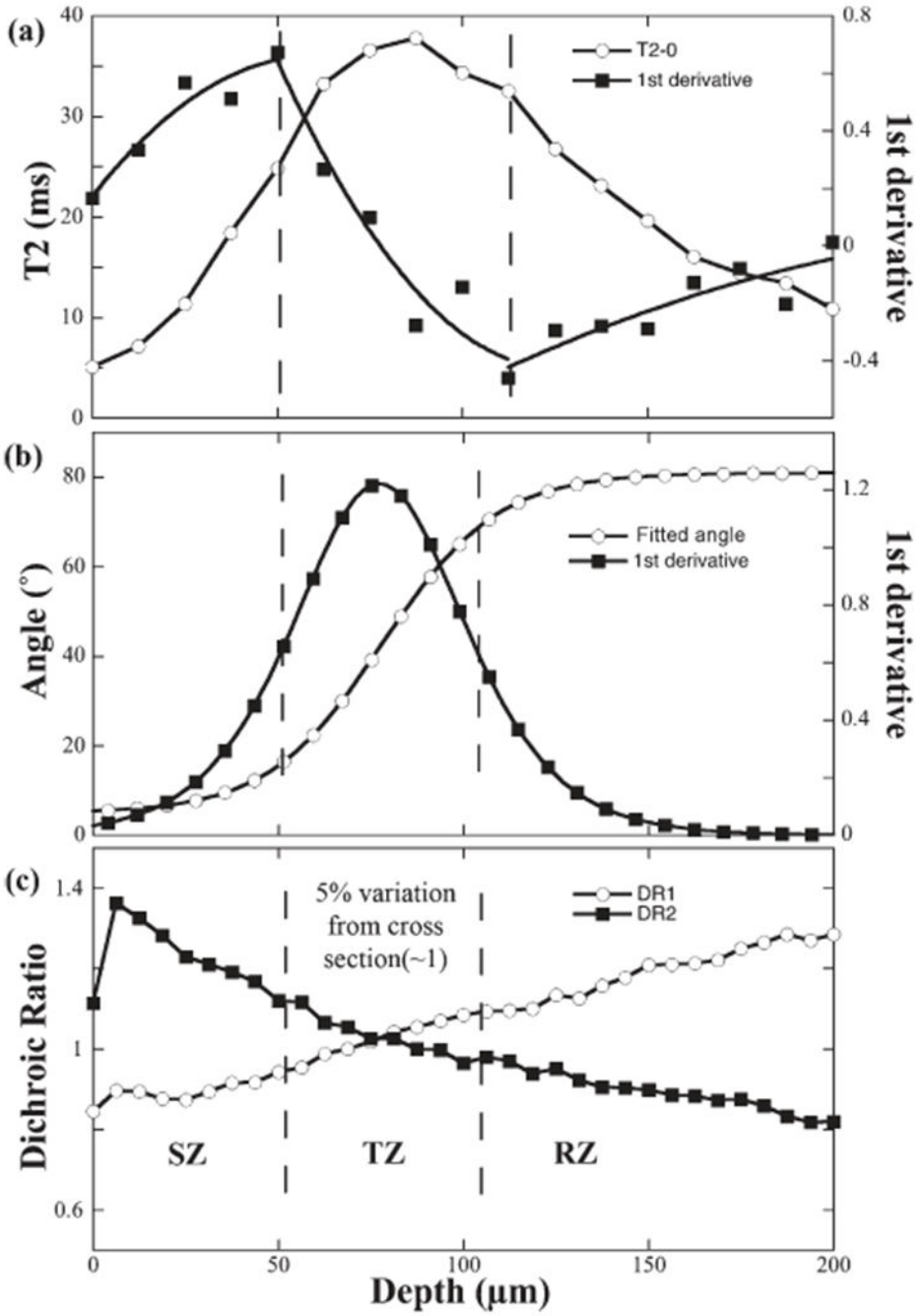

Fig. 4.

The criteria that define the location and thickness of the TZ in microscopic imaging (an enlarged view of the profiles in Fig 3). **a:** The profiles of the T_2 and the first derivative of T_2 at 0°. **b:** The profiles of the fitted angle and the first derivative of angle (Only one in every 10 pixels was plotted). **c:** The profiles of the dichroic ratios for amide I (DR1) and amide II (DR2).

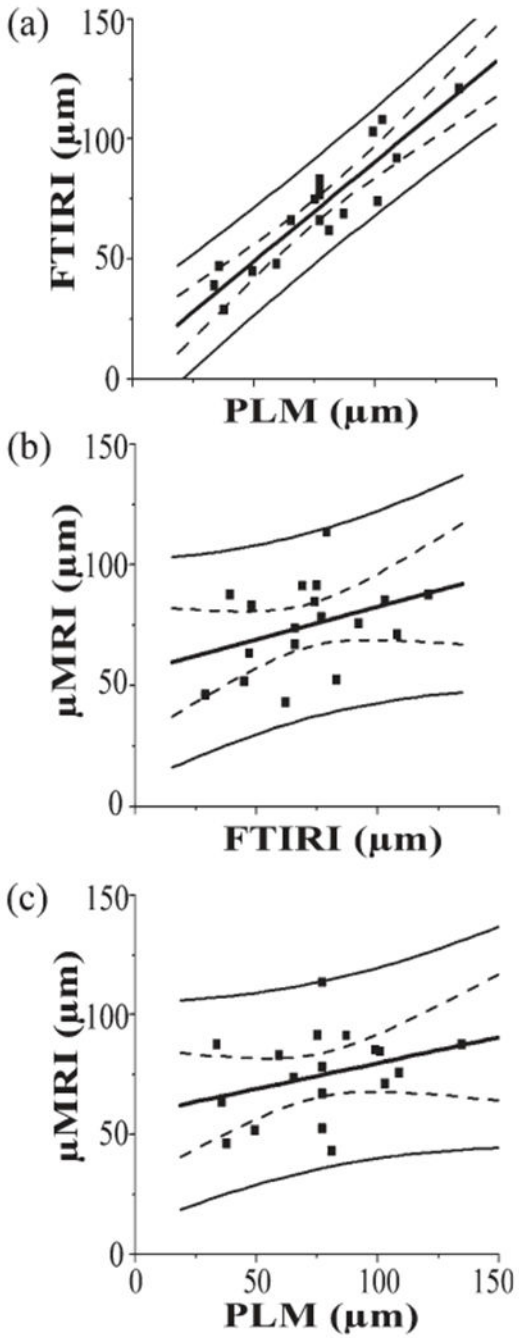

Fig. 5.

The linear correlations of the most random locations between (**a**) FTIRI and PLM, (**b**) μMRI and FTIRI, and (**c**) μMRI and PLM. The solid curves showed the 95% confidence intervals for individual points and the dotted curves showed the 95% confidence interval curve for the means. The r values and correlation probabilities in the fitting were (a) $r = 0.9192$ and $P < 0.0001$, (b) $r = 0.3477$ and $P = 0.1574$, and (c) $r = 0.2926$ and $P = 0.2387$.

TABLE 1.

Characteristics of articular cartilage from canine humerus (N = 18)

Techniques	Parameters	Values
μMRI	Value of max T_2 at 0° (ms)	43 ± 5
	Depth of max T_2 at 0° (μm)	83 ± 19
	Ave T_2 at 55° (ms)	47 ± 6
	Ave $T_{1\text{-before}}$ at 55° (s)	1.1 ± 0.1
	Ave GAG (mg/mL)	74 ± 22
PLM	Depth of Retardation min (μm)	80 ± 25
	Value of Retardation min (nm)	0.7 ± 0.2
FTIRI	Depth of DR crossing (μm)	71 ± 25
	Value of the DR crossing	1.0 ± 0.1

TABLE 2.

Multidisciplinary criteria for the zone division

	μMRI	PLM	FTIRI
The central feature	The zero-crossing of the first derivative of T_2 at 0°	The peak of the 1st derivative of angle hyperbolic tangent	The cross-point of DR Amide I and DR Amide II
Criteria for the TZ	From max to min of the first derivative of T_2 at 0°	FWHM on each slope of the central peak	5% variation from the crossing point
Criteria for the total thickness	Use the boundaries of cartilage with the saline (S1) and the bone (S2) in the proton map at 55°	From the articular surface to the top of the lower boundary between the tissue and bone based on the angle images.	Use the high resolution visible images
Independent parameters	(1) the total thickness of the cartilage, (2) the location of the transitional zone, (3) the thickness of the transitional zone		

TABLE 3.

Correlations of the subtissue zones in articular cartilage (N = 18)

	μMRI	PLM	FTIRI	*P*[a]
Total tissue (μm)	669 ± 62	646 ± 49	626 ± 65	0.106
SZ thickness (μm)	42 ± 13 (44 ± 13)	51 ± 22 (46 ± 22)	48 ± 21 (56 ± 22)	0.376
TZ thickness (μm)	62 ± 16 (81 ± 12)	54 ± 18 (63 ± 14)	52 ± 9 (36 ± 9)	0.117
RZ thickness (μm)	555 ± 68 (544 ± 69)	542 ± 67 (537 ± 66)	526 ± 73 (626 ± 65)	0.260
Depth of the most random location in AC (μm)	75 ± 18	77 ± 27	71 ± 25	0.783

The tissue thickness from the previous criteria is shown in the bracket.

[a]The *P*-values (95%) of One-Way ANOVA with Bonferroni correction among three criteria (i.e., three imaging methods).